Denitrification kinetics during aquifer storage and recovery of drainage water from agricultural land

Kruisdijk, Emiel; Eisfeld, Carina; Stuyfzand, Pieter J.; van Breukelen, Boris M.

DOI
10.1016/j.scitotenv.2022.157791

Publication date
2022

Document Version
Final published version

Published in
Science of the Total Environment

Science of the Total Environment 849 (2022) 157791

Contents lists available at ScienceDirect

Science of the Total Environment

journal homepage: www.elsevier.com/locate/scitotenv

Denitrification kinetics during aquifer storage and recovery of drainage water from agricultural land

Emiel Kruisdijk [a,b,*], Carina Eisfeld [a], Pieter J. Stuyfzand [a,c], Boris M. van Breukelen [a]

[a] Delft University of Technology, Faculty of Civil Engineering and Geosciences, Department of Water Management, Stevinweg 1, 2628 CN Delft, the Netherlands
[b] Acacia Water B.V., Van Hogendorpplein 4, 2805 BM Gouda, the Netherlands
[c] Stuyfzand Hydroconsult+, 2042 BL Zandvoort, the Netherlands

HIGHLIGHTS

- Denitrification was assessed before and during ASTR operation.
- Three different types of in-situ field monitoring approaches were executed.
- A ~6-day denitrification lag-phase was observed during the push-pull tests.
- Rate constants increased probably due to microbial adaptation and bioaugmentation.
- Higher rate constants were observed during injection compared to storage.

GRAPHICAL ABSTRACT

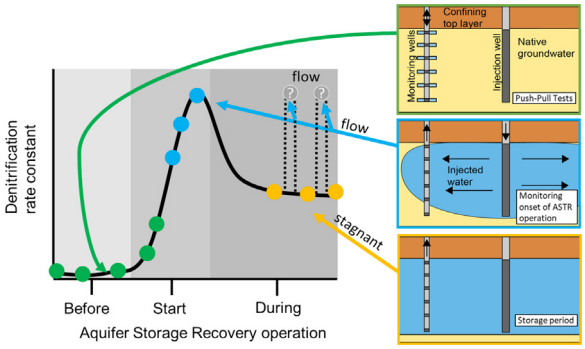

ARTICLE INFO

Editor: José Virgílio Cruz

Keywords:
Denitrification
Aquifer storage and recovery
Managed aquifer recharge
Monitored natural attenuation
Agriculture
Bioaugmentation

ABSTRACT

An aquifer storage transfer and recovery (ASTR) system was studied in which tile drainage water (TDW) was injected with relatively high NO_3 (about 14 mg/L) concentrations originating from fertilizers. Here we present the evolution of denitrification kinetics at 6 different depths in the aquifer before, and during ASTR operation. First-order denitrification rate constants increased over time before and during the first days of ASTR operation, likely due to microbial adaptation of the native bacterial community and/or bioaugmentation of the aquifer by denitrifying bacteria present in injected TDW. Push-pull tests were performed in the native aquifer before ASTR operation. Obtained first-order denitrification rate constants were negligible (0.00–0.03 d^{-1}) at the start, but increased to 0.17–0.83 d^{-1} after a lag-phase of about 6 days. During the first days of ASTR operation in autumn 2019, the arrival of injected TDW was studied at 2.5 m distance from the injection well. First-order denitrification rate constants increased again over time (maximum >1 d^{-1}). Three storage periods without injection were monitored in winter 2019, fall 2020, and spring 2021 during ASTR operation. First-order rate constants ranged between 0.12 and 0.61 d^{-1}. Denitrification coupled to pyrite oxidation occurred at all depths, but other oxidation processes were indicated as well. NO_3 concentration trends resembled Monod kinetics but were fitted also to a first-order decay rate model to facilitate comparison. Rate constants during the storage periods were substantially lower than during injection, probably due to a reduction in the exchange rate between aquifer solid phases and injected water during the stagnant conditions. Denitrification rate constants deviated maximally a factor 5 over time and depth for all in-situ measurement approaches after the lag-phase. The combination of these in-situ approaches enabled to obtain more detailed insights in the evolution of denitrification kinetics during AS(*T*)R.

* Corresponding author at: Delft University of Technology, Faculty of Civil Engineering and Geosciences, Department of Water Management, Stevinweg 1, 2628 CN Delft, the Netherlands.
E-mail address: e.kruisdijk@tudelft.nl (E. Kruisdijk).

http://dx.doi.org/10.1016/j.scitotenv.2022.157791
Received 25 April 2022; Received in revised form 25 July 2022; Accepted 30 July 2022
Available online 6 August 2022

1. Introduction

Nitrate (NO_3) pollution is an environmental problem worldwide, to which agricultural fertilizers are contributing largely. Camargo and Alonso (2006) reviewed the ecological and toxicological hazards in aquatic environments. They summarized that NO_3 contamination induces risks of acidification and eutrophication. Furthermore, toxic levels affect the survival, growth, and reproduction of animals. Human exposure to NO_3 polluted drinking water is linked to methemoglobinemia and cancers (Wolfe and Patz, 2002).

In groundwater, NO_3 is the most prevalent contaminant in the world (Korom, 1992). It is highly soluble and therefore spreads easily during advective transport. Fortunately, transformation can significantly decrease NO_3 concentrations in aquifers. Bacterial communities use NO_3 as an electron acceptor within their metabolic processes, and thereby convert it through different steps to the non-polluting N_2 gas (Appelo and Postma, 2004). The latter process, called denitrification, is largely depending on available electron donors and environmental conditions such as O_2 and NO_3 concentrations (Antoniou et al., 2012; Korom et al., 2005), nutrient and micro-nutrient availability (Hunter, 2003; Kowalenko, 1979), pH (Rust et al., 2000), temperature (Prommer and Stuyfzand, 2005), salinity (Henze and Ucisik, 2004), inhibitory substances (Sáez et al., 2006), sediment pore size (Blakey and Towler, 1988), microbial adaptation (Ghafari et al., 2009), and flow rate (Gorski et al., 2020; Schmidt et al., 2011). Generally, denitrification is likely to occur in aquifers, if electron donors are present, although rates vary greatly (Korom, 1992).

Aquifer Storage and Recovery (ASR) is a well injection technique used to store water in aquifers for later abstraction using the same well (Pyne, 1995). Aquifer Storage Transfer and Recovery (ASTR) is a similar technique, where different wells are used for injection and abstraction to create a minimum distance for aquifer passage. Injected and stored water can originate from, for example, treated wastewater (e.g., Sheng, 2005; Vanderzalm et al., 2020), surface water (Jones and Pichler, 2007), or as in the current study: tile drainage water (Kruisdijk and van Breukelen, 2021). These waters can have substantial NO_3 concentrations. Therefore, understanding denitrification in AS(*T*)R systems is crucial to assess the risk of groundwater contamination, the water quality of the reused AS(*T*)R water, and potential emissions of the greenhouse gas N_2O (which is a transformation by-product during denitrification).

Several methods have been used to study denitrification in AS(*T*)R systems. Mass balance approaches were used in various studies to calculate the percentage removal of NO_3 (Antoniou et al., 2012; Vanderzalm et al., 2020; Vanderzalm et al., 2013). Reactive transport models were used to estimate reaction rates of processes, like pyrite and organic matter oxidation, which are partly responsible for denitrification (Antoniou et al., 2013; Greskowiak et al., 2005). In all above-mentioned studies, NO_3 fate was examined based on operational monitoring data, which generally consists of the injected and abstracted water composition and the composition observed in monitoring wells at different depths and distances from the injection well obtained at various moments in time. Therefore, the obtained insights on denitrification are based on relatively long periods (16–± 800 days).

In the current study, we focus on 3 different approaches to determine in-situ denitrification rate constants performed during several shorter periods (6–46 days) before and during ASTR, which were monitored with a high frequency. Monitoring at 6 different depths enabled us to assess intra-aquifer variations of denitrification kinetics and rate constants. First-order and Monod denitrification rate constants were obtained from 5 periods (before operation, at the start of operation, and 3 times during operation) and were used to assess the evolution of denitrification rates over time. This is meaningful as a denitrification lag-phase can occur at the start of ASTR operation until the aquifer sets to a new equilibrium, which is achieved after the aquifer is microbially adapted to the new water source (Korom, 1992; Rivett et al., 2008) and bioaugmented by the bacteria in the injected water (Lyon and Vogel, 2013). This is to our knowledge never studied before. Moreover, during ASTR operation denitrification can decrease due to depletion of electron donors like pyrite or sedimentary organic matter (Antoniou et al., 2013). Objectives of this research were to: (i) examine the lag-phase of denitrification related to microbial adaptation and bioaugmentation at the start of ASTR operation, (ii) assess the denitrification kinetics and rate constants before and during ASTR operation, and (iii) analyze the variation in denitrification rates over time and with depth and its relation to available electron donors. Finally, we describe the potential benefits of studying ASTR systems with the in-situ field methods proposed in this study.

2. Methods

2.1. Field site description

This study is performed at an agricultural Aquifer Storage Transfer and Recovery (ASTR) system located in an agricultural polder in the North-Western part of the Netherlands (coordinates: 52.8883, 4.8221). The ASTR system collects water from a tile drainage network approximately 1 m below a 10 ha agricultural parcel. This drainage network normally discharges water to the surface water, but in this system all tile drains end up in a collection drain, which discharges the tile drainage water (TDW) to the ASTR system. As the TDW comprises nutrients and pesticides, the load of these agrochemicals to the surface water system is substantially reduced.

TDW is injected by 2 injection wells into a deeply anoxic, semiconfined sandy aquifer (11.5–33.0 m below surface level (b.s.l)) of late Holocene and Pleistocene age, below a confining Holocene clay/peat layer. In dry periods, water is abstracted by 4 abstraction wells (12.0–23.0 m b.s.l.) for irrigation of the agricultural crops. During ASTR operation, injected volumes were monitored for each injection event. A set of 6 monitoring wells is located at 2.5 m distance from injection well A (Fig. 1), with well screens of 1 m located at different depths ranging from 11.4 to 32.2 m-b.s.l.

2.2. Description of push-pull tests

Push-pull tests (PPTs) were performed at the 6 monitoring wells (MW1-MW6) located at 2.5 m distance from injection well A before the onset of ASTR operation, from 25 February 2019 till 18 March 2019. The method is similar to the one applied by Kruisdijk and van Breukelen (2021). Samples were taken from the native groundwater before the PPTs. During the PPTs, water with known composition is injected through a monitoring well into the aquifer ('push'-phase), after which the injected water is gradually abstracted and sampled ('pull'-phase). About 300 L TDW was used as injection water and stored in a 500 L tank. In this tank, a conservative tracer was added (0.1 mmol/L Br as NaBr) and a reactant (~50 mg/L NO_3, as $NaNO_3$), after which the water was thoroughly mixed manually with a pole. Per monitoring well, a storage tank was prepared for injection. Injection occurred with a steady flow of about 2 L/min for approximately 2.5 h, during which four water samples were taken equally distributed over the injection time. Afterwards, the water was periodically abstracted, and water samples were taken. The first water sample was taken after about 4 h of storage following injection. Subsequently, 11 more samples were taken, each after abstraction of 30 L (maximum standing volume of wells: 17 L). The time in between sampling slowly increased from 4 h to three days between the last two samples. Before taking the last two samples, 60 L was abstracted instead of 30 L. The total duration of the PPTs was 17–18 days and a total of 480 L was abstracted. The concentrations obtained from the analyzed water samples were used to determine first-order denitrification rate constants, based on the well-mixed reactor model (Haggerty et al., 1998).

2.3. Monitoring the onset of ASTR operation

2.3.1. Method

The onset of ASTR operation was frequently monitored from 2 till 6 November 2019. In this period, a total of 440 m^3 natural TDW was injected.

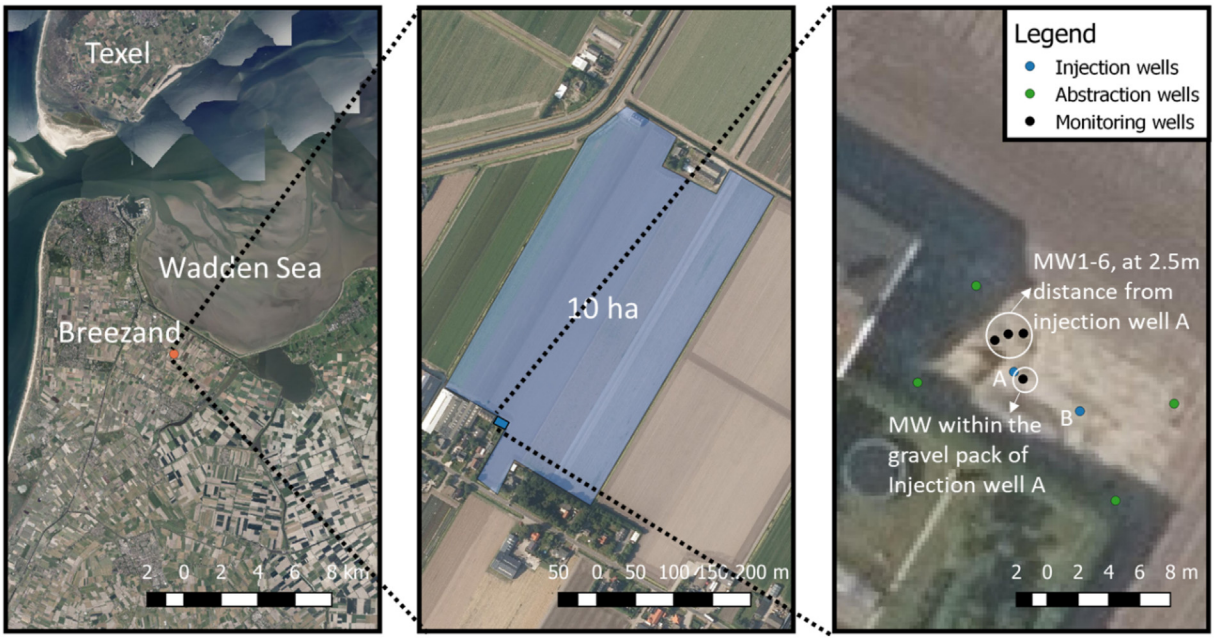

Fig. 1. Top view of the field site location in Breezand, the Netherlands. The orange dot in the left panel shows the ASTR system location in the NW Netherlands. The middle panel shows the agricultural field from which tile drainage water is collected in light blue. The ASTR system location is shown in dark blue. This part is shown in more detail in the right panel, where the blue dots represent injection well A and B, the green dots the 4 abstraction wells and the black dots the boreholes of the monitoring wells. The 3 boreholes at 2.5 m distance from the injection well, each consist of 2 monitoring wells (=6 monitoring wells (MW1-6)). The black dot next to injection well A represent the monitoring well within the gravel pack of this injection well. Adapted from Kruisdijk and van Breukelen (2021).

Injected TDW contained NO_3 from agricultural fertilizers. TDW arrival was monitored at the 6 MW at 2.5 m distance from injection well A. ASTR injection was set to only occur during daytime. Cl concentrations acted as a natural tracer, as concentrations in TDW were substantially lower than in native groundwater. Injected TDW composition was monitored by taking water samples from the monitoring well within the gravel pack of injection well A every 30 min. The internal volume of this monitoring well was purged at the start of each day (about 60 L was abstracted, standing well volume: ca. 11 L). Simultaneously, each of the 6 MW was sampled with a time interval of 3 h. Before each sample, the standing volume of the well (max. 17 L) was purged by abstracting 30 L using a diaphragm pump (Liquiport NF1.100, KNF Verder, the Netherlands).

2.3.2. Data analysis

First-order denitrification rate constants were examined using a 1-D radially axisymmetric solute transport model. A model was set up for each well screen depth, assuming horizontal flow only (neglecting regional lateral flow), as induced by injection. The model was developed using PHREEQC (Parkhurst and Appelo, 2013). It consisted of 300 cells of varying lengths to simulate radial flow, as done before by, e.g., Bonte et al. (2014) and Antoniou et al. (2013). Every cell represents the same volume. As the injection flow is stable, the timestep is constant for each transport shift from one cell to the next. The timestep can therefore be determined by dividing the injection time till the arrival of the spreading front at the monitoring well by the number of cells. The injection periods were simulated as forward flow transport steps, from which the number of shifts were determined by dividing the hours of injection by the timestep. In the periods without injection, stagnant conditions were simulated without diffusion. In each model, denitrification was simulated with first-order rate constants of 0.0, 0.25, 0.5 and 1.0 d^{-1}. Simulated and observed NO_3 concentrations were plotted and visually compared to obtain insights in the first-order rate constants at the different depths during the onset of ASTR operation. Furthermore, conservative concentrations (concentrations only affected by advection and dispersion) were simulated, plotted, and visually compared with observed NO_3, SO_4, Fe, and DOC concentrations.

2.4. Description of storage period monitoring

2.4.1. Method

Injection did not occur continuously during ASTR operation, due to periods of droughts or system maintenance. Periods without injection are here referred to as storage periods. In these periods injected TDW was assumed to be stagnant, which was considered acceptable as (i) background groundwater flow velocity is negligible at only max. 0.01 m/d, based on groundwater levels and hydraulic conductivity in the area (groundwater levels from www.grondwatertools.nl; hydraulic conductivity from www.dinoloket.nl), and (ii) natural tracer concentrations (Cl concentrations) were relatively stable during the storage periods (Supplementary Information 3.2 (S3.2)). Periodically, a storage period was monitored to assess denitrification. During the storage periods, water samples were taken repeatedly from different aquifer depths via the monitoring wells. Before every sample, 1.5× the internal volume of the monitoring well was abstracted.

The aquifer volume (sediments + pores) investigated can be calculated by:

$$V_{total} = \frac{V_{abstracted} - V_{internal\ volume}}{n} \quad (1)$$

where $V_{abstracted}$ is the volume abstracted (m^3), $V_{internal\ volume}$ is the internal volume of the monitoring well (m^3), and n is the porosity (dimensionless), which was assumed to be 0.3. If we assume a cylindrical portion of the aquifer for $V_{abstracted}$, a corresponding radius can be calculated by the equation proposed by Istok (2012):

$$r = \sqrt{\frac{V_{total}}{\pi h}} \quad (2)$$

where r is the radius (m), and h is the length of the monitoring well screen (m). Based on this calculation, the radius of the total abstracted water during storage period 1 (6 samples) was between 0.23 and 0.37 m, for

storage period 2 (12 samples) 0.34–0.54 m, and for storage period 3 (8 samples) between 0.27 and 0.44 m.

2.4.2. Obtaining rate constants

Observed concentrations were plotted versus the time elapsed since the first measurement of each storage period measurement. First-order rate constants were obtained by using a least-squares routine to fit a first-order expression regression line to the observed concentrations in python (Python v. 3.6.4). Monod kinetic parameters (V_{max} and K_s) were obtained by fitting the observed concentration to an explicit expression proposed by Schnell and Mendoza (1997).

2.5. Hydrochemical and geochemical analysis

In the field, water quality was sensed for pH and temperature (PHEHT, Ponsel, France), and dissolved oxygen (OPTOD, Ponsel, France) using a flow cell. Furthermore, water samples were taken and on site filtered (0.45 μm, Chromafil Xtra PES-45/25, Macherey-Nagel, Germany). They were analyzed for dissolved anions (Br, Cl, NO_3, and SO_4) with Ion Chromatography (IC; Compact IC pro, Metrohm, Switzerland). Fe was analyzed with Inductively Coupled Plasma – Mass Spectrometry (ICP-MS; PlasmaQuant MS, Analytik-Jena, Germany). Alkalinity, and NH_4 were measured with a Discrete analyzer (DA; AQ400, Seal analytical, UK). Dissolved organic carbon (DOC) was determined with a TOC analyzer (TOC-V CPH, Shimadzu, Japan).

Prior to installation of MW1-6, sediment samples were obtained from the boreholes using a 2 m sonic drill aqualock system with a core catcher. The reader is referred to the Supplementary Information (S4) for more details on the sediment sampling. The sediment samples were analyzed by high temperature combustion with non-dispersive infrared detection for sedimentary organic carbon (SOC), thermogravimetric analysis for carbonate mineral content, and x-ray fluorescence after lithium borate fusion for S contents. The median grainsize (D50) was obtained by a HELOS/KR laser particle sizer (Sympatec GmbH, Germany) after removal of sedimentary organic matter and carbonates. Pyrite contents were estimated from the total S content:

$$FeS_2 = 0.5(M_{FeS_2}/M_s)S \quad (3)$$

where M_i is the molecular weight of i (g/mol), S is the sulphur content (% d.w.). The total S content is assumed to be originating from pyrite, as done before for Dutch sediments by e.g., Zuurbier et al. (2016) and Bonte et al. (2013).

2.6. Analysis of bacterial community by 16S rRNA analysis

Samples were collected in autoclaved 1 L bottles and filtered using Nalgene Reusable Filter units (Thermo Scientific). Bacterial cells were collected onto 0.22 μm polycarbonate filters (Merck Millipore) and onto 0.45 μm filters in 2019. Samples were taken and analyzed for the bacterial community compositions of: (i) native groundwater in 2019 before ASTR operation, (ii) TDW, sampled weekly for 5 weeks during the Fall 2020 storage period, (iii) groundwater during the Fall 2020 storage periods. Groundwater samples were taken from MW1–6, after abstraction of 3× the standing well volume. The filters with biomass were stored at −20 °C until DNA extraction. For DNA extraction, filters with the biomass were disintegrated using Powerbead tubes (Qiagen) and the environmental DNA was extracted with the DNeasy PowerLyzer PowerSoil Kit (Qiagen) following the manufacturer's instructions. Extracted DNA was quantified in the Qubit 4 Fluorometer (Thermofisher), and the extracted DNA samples were sent to Novogene (Hong Kong) for 16S ribosomal RNA (rRNA) sequencing. The V3-V4 hypervariable region was targeted using the universal primers 341F (5′- CCT ACG CGA GGC AGC AG) (Miettinen et al., 2015; Muyzer et al., 1993; Shu et al., 2016) and sequenced with Illumina HiSeq paired-end platform to generate paired-end raw reads of 400–450 bp. Data analysis was performed using the programming language R (version 4.1.2) (team RC, 2013) and the Vegan package (Oksanen et al., 2013).

3. Results

3.1. Aquifer storage transfer and recovery operation

In total, about 10,000 m^3 water was injected equally spread over injection well A and B during ASTR operation. No abstraction took place during the period of investigation. Before operation period 1, push-pull tests (PPTs) were performed from 25 February 2019 till 18 March 2019. From 2 till 6 November 2019, the onset of ASTR operation was monitored. The first storage period was performed in the winter of 2019 after operation period 1, during which approximately 2700 m^3 water was injected combined over both injection wells. The storage period was repeated after operation period 2 in fall 2020 and after operation period 3 in spring 2021, during which respectively 2900 m^3 and 4300 m^3 water was injected. An overview of the Aquifer Storage Transfer and Recovery (ASTR) operation, injected volumes, and the different monitoring approaches and events is shown in Supporting Information 1 (S1). The mean NO_3 concentration in injected tile drainage water (TDW) between 25 February 2019 and 18 March 2021 was 14.1 ± 11.3 mg/L.

3.2. Push-pull tests

Observed conservative NaBr tracer concentrations show a gradual transition from TDW to native groundwater levels during the 'pull'-phase (abstraction) of the push-pull tests (PPTs), due to hydrodynamic dispersion (S2.1). O_2 concentrations in the injected water were on average 6.8 mg/L ± 1.4 mg/L, and were generally reduced to <0.2 mg/L within 1 day after injection. First-order aerobic respiration and denitrification rate constants were calculated using the well-mixed reactor model (Haggerty et al., 1998). Observations were only used for analysis when their solution contained >20 % TDW, which was calculated based on tracer concentrations. The obtained aerobic respiration rate constants were substantially less reliable than those of denitrification, as they were only based on 2 measurements (the injected concentrations plus one observation) (S2.2). The first-order rate constants ranged from 19 to 39 d^{-1}. At MW1 and MW3, O_2 concentrations remained below the detection limit (0.2 mg/L), which resulted in a minimum first-order rate constants of >83 and >44 d^{-1} for MW1 and MW3, respectively.

Fig. 2 displays the calculated first-order denitrification rate constants. Denitrification was negligible or insignificant at all depths during the first 5–6 days (max. k_A = 0.06 d^{-1}). The calculated k is denominated statistically significant if the confidence interval of the DT50 excludes k = 0, which only applied for MW6. After the first 5–6 days, denitrification was observed with rate constants between 0.17 and 0.83 d^{-1} (k_B). Highest denitrification rate constants were observed at MW2 and MW3, respectively 0.83 and 0.54 d^{-1}. However, note that these rate constants are less accurate, as they are obtained from only 2 or 3 measurements (injected concentrations not included). We expect that the remarkable change in denitrification rate constants after 5–6 days is resulting from microbial adaptation and/or bioaugmentation.

3.3. The onset of ASTR operation monitoring

Arrival of injected TDW was monitored at the well screen depths of MW1–6 during the first 6 days of ASTR operation (Fig. 3). Cl concentrations were lower in injected TDW than in the native brackish aquifer at all depths. Therefore, observed Cl concentrations decreased gradually as the ASTR injected TDW passed by the monitoring wells. ASTR operational data and Cl concentrations were used to determine the travel time and the injected volume of water needed for the arrival of the spreading front at the different depths (S4.1). Substantial variations were observed at the different depths, for example the earliest arrival occurred at MW4 after injection of 110 m^3, and the latest at MW6 after injection of 423 m^3.

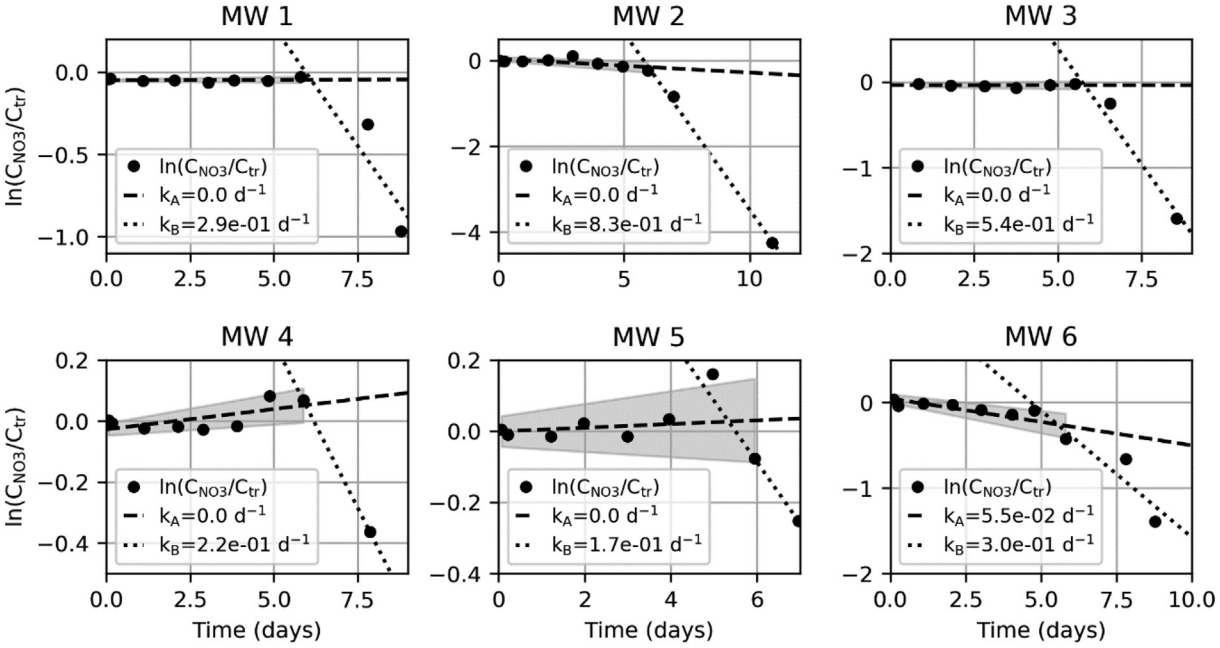

Fig. 2. First-order denitrification rate constants calculated at the different well screen depths during the PPTs, with on the y-axis the natural logarithm of the observed NO_3 concentrations divided by the tracer concentrations, and on the x-axis the days after injection. The dashed line presents the linear trendline for all samples till 6 days (k_A), and the dotted line for samples after 5 days (k_B). The slope of these lines represents the denitrification rate constants. The grey area behind the fitted line for the first 6 days represents the 95 % confidence intervals, which is shown to assess the significancy of kA. kA was set to 0.0 when insignificant.

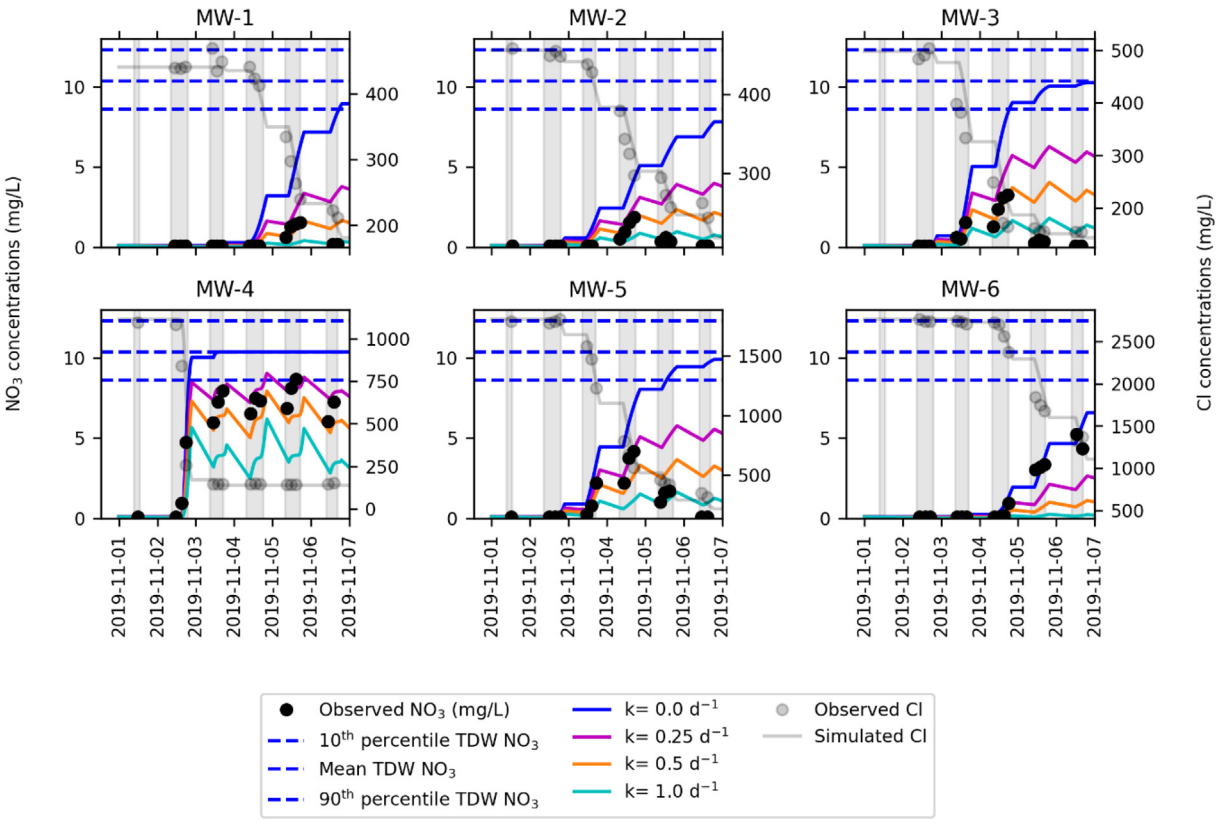

Fig. 3. Observed and simulated NO_3 and Cl concentrations during monitoring of the onset of ASTR operation. The black dots present the observed NO_3 concentrations, and the grey dots the Cl concentrations. The grey line shows the simulated Cl concentrations. The different color lines present the simulated NO_3 concentrations with various first-order denitrification rate constants. The dashed blue lines show the minimum, mean, and maximum observed NO_3 concentrations in TDW. The grey vertical bars in the background show the periods during which injection occurred.

The arriving TDW did not contain detectable O_2 at all depths (results not shown). This indicates that O_2 was fully depleted during aquifer transport, from injection well A to the monitoring wells, in <1 day. This agrees with the O_2 consumption at the PPTs. NO_3 was significantly reduced at MW1-5, as shown by the lower NO_3 concentrations after arrival compared to the injected water, but not at MW6. A simplified 1-D advection-dispersion model was set up in PHREEQC, which simulates the onset of ASTR operation. Different first-order denitrification rate constants were simulated in the model, which enabled us to compare observed and simulated NO_3 concentrations and relate the observed concentrations to the applicable first-order rate constants. Fig. 3 shows the observed Cl and NO_3 concentrations and the simulated model fits. A good fit was observed between observed and simulated Cl concentrations at all depths, which indicates that the model simulates ASTR operation sufficiently well. During the first 4 days, the observed NO_3 concentrations correspond with first-order denitrification rate constants of about 0.25–0.5 d^{-1} at the well screen depths of MW1-5. Afterwards, denitrification rate constants increase to >1.0 d^{-1} at MW-1,2,3 and 5 in the following 2 days. The increased denitrification rate constants caused most observed NO_3 concentrations to decrease below the detection limit. Microbial adaptation and bioaugmentation likely control the increased denitrification rate constants during the onset of ASTR operation.

After the first 6 days of ASTR operation, injection did not occur for two weeks, and water samples were taken after about 2 and 12 days of the stagnant water at all depths (S3.1). NO_3 concentrations were already depleted at most depths, except at MW4 and MW6. At MW4, an increased denitrification rate constant was observed ($\pm$1.0 d^{-1}) compared to during injection (0.25 d^{-1}), while denitrification eventually did kick in at MW 6 during this subsequent storage phase with a rate constant of $\pm$0.1–0.5 d^{-1}.

3.4. Storage periods

3.4.1. Obtained rate constants

Three storage periods were monitored after periods of injection wherein substantial volumes of TDW were injected (2700–4300 m^3). Fig. 4 presents observed NO_3 concentrations and the fitted first-order decay rate models at the different depths during the three storage periods. NO_3 concentrations decreased over time at all different depths during all storage periods, which indicated occurrence of ongoing denitrification. At the onset of the storage periods, NO_3 concentrations varied at the different depths because of (i) the variations in travel times from injection well to the monitoring wells, (ii) the slightly varying denitrification rate constants at each depth, and (iii) the variation of NO_3 concentrations in injected TDW over time. Generally, highest NO_3 concentrations were observed during the fall 2020 storage period, and lowest during the spring 2021 storage period. NO_3 was already fully reduced before arrival at MW6 (having the longest travel time), but also during the winter 2019 storage period at MW3, and the spring 2021 storage period at MW2.

NO_3 concentration trends resembled Monod (or Michaelis-Menten) kinetics, where at high concentrations denitrification approaches pseudo zero-order kinetics and at low concentrations pseudo first-order kinetics (Bekins et al., 1998; Breukelen and Prommer, 2008). At concentrations >5 mg/L, NO_3 concentrations followed mostly zero-order kinetics, as observed at MW1, 4, and 5. Denitrification rates slowed down and followed pseudo first-order kinetics at concentrations <5 mg/L. Monod kinetic parameters (V_{max} and K_s) were fitted to the data but often could not be accurately determined (S4.3). The measurements were unequally distributed over the pseudo zero- and first-order part, which resulted in an insufficient number of measurements for an accurate fit. Nevertheless, accurate V_{max} (fitted on >3 measurements on the pseudo zero-order part (>5 mg/L))

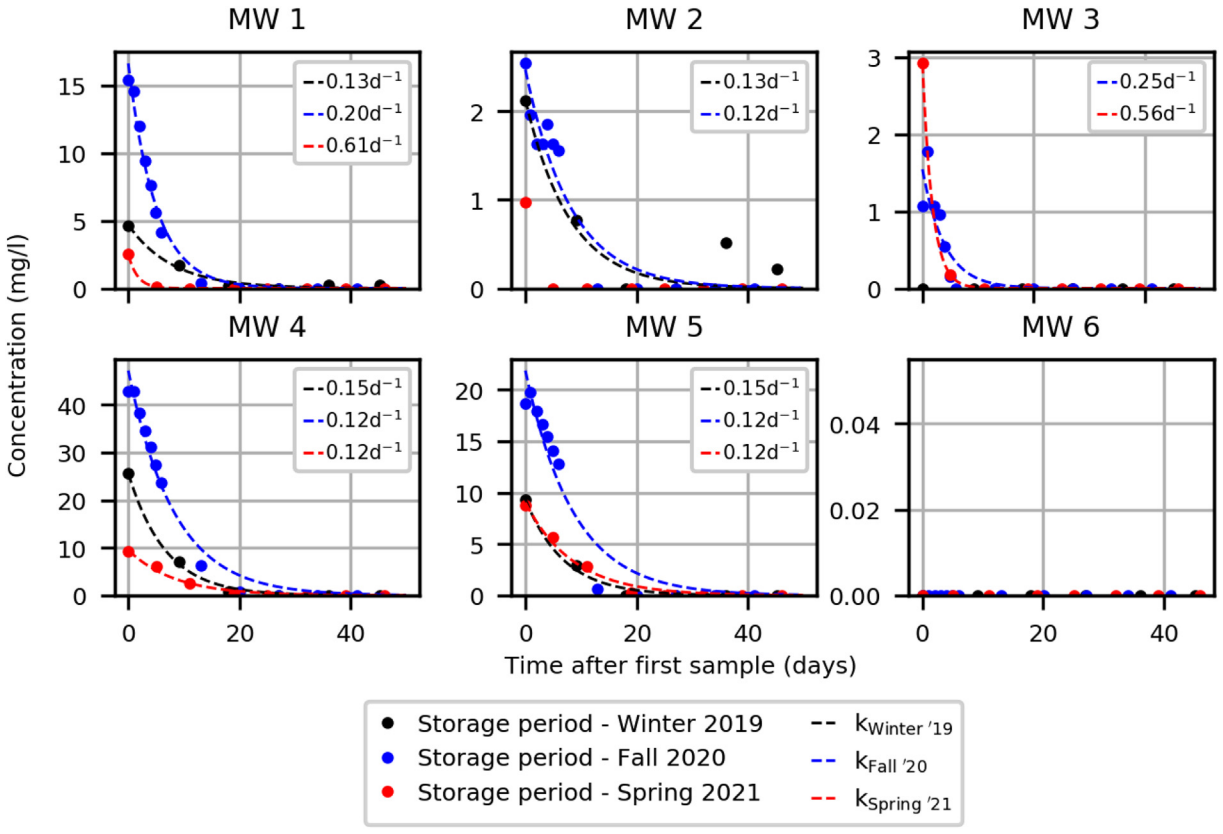

Fig. 4. Observed NO_3 concentrations and the obtained first-order denitrification rate constants during the three storage periods at all well screen depths. The dots present the observed concentrations, the dashed lines the fitted first-order decay rate models.

were determined at the screen depths of MW1, 4, and 5 for the Fall 2020 storage period. A higher V_{max} was observed at MW4, compared to MW1 and 5 (MW1: 1.92; MW4: 3.21; MW5 1.21 mg/ L d^{-1}).

We also decided to fit simpler first-order kinetics (only 1 fitting parameter, instead of 2 by Monod kinetics) to the observed NO_3 concentrations, as the obtained Monod kinetic parameters were often inaccurate. Better visual fits are observed, although the rate constants seem to generally underestimate denitrification at the lower concentrations in the Fall 2020 storage period (Fig. 4). Obtained denitrification rate constants are similar, between 0.12 and 0.25 d^{-1}, for fits with >2 NO_3 measurements above detection limit. At MW1 and MW3, higher rate constants are observed (0.61 and 0.56 d^{-1}, respectively), but these rate constants are fitted on only two measurements. We did not obtain a higher first-order rate constant at MW4 compared to MW1 and 5 during the fall 2020 storage period, contrary to the obtained V_{max}.

3.5. Bacterial communities in native groundwater, TDW, and groundwater during ASTR operation

The bacterial communities of the native groundwater before ASTR, TDW, and groundwater during ASTR operation (during the fall 2020 storage period) were analyzed using 16S rRNA analysis. A total of 1810 operational taxonomic units (OTU's) were detected in all the collected samples. Genera were considered relevant that were on average >1 % abundant or had a peak in relative abundance of >5 %. The bacterial community of the native groundwater (Fig. 5B) was distinctively different compared to TDW (Fig. 5A). The main genera in TDW remained rather constant and were composed of *Gallionella*, *Sulfurimonas* and *Sulfuricurvum*. Note, that the chemical and biological composition of the TDW can vary over the year, due to changing agricultural practices and influences of the weather. The native groundwater showed an overall similar bacterial community at the different depths, but slight variations between the communities were observed. Before the fall 2020 storage period, >5000 m^3 TDW was injected. The aquifer community changed greatly (Fig. 6C) and resembled more to the TDW community.

Spearman rho statistics were applied to test the strength of association between the bacterial community of the groundwater during ASTR operation, TDW, and native groundwater samples (Table 1). This showed that the groundwater during ASTR operation was strongly influenced by the bacterial community of the TDW represented by high ρ = 0.80–0.85. In contrast, the relation between native groundwater before injection and TDW was represented by lower ρ (0.38–0.49).

4. Discussion

4.1. Evolution of denitrification rate constants during ASTR

4.1.1. Increasing rate constants during PPTs and during the onset of ASTR operation

First-order denitrification rate constants increased at almost all depths during the PPTs and during monitoring of the onset of ASTR operation.

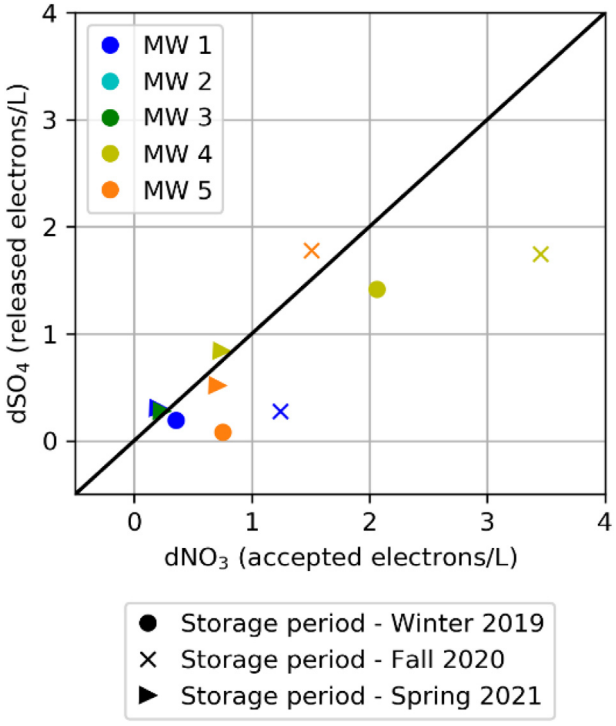

Fig. 6. Electrons released by the formation of SO_4 during pyrite oxidation versus the electrons accepted during denitrification. The different colors present the depths in the aquifer, and the different marker types the period in which the storage period is performed. The linear black line indicates a 1:1 ratio of released and accepted electrons. NO_3 concentration < 2 mg/L at the start of the storage period were discarded, as large uncertainties could result of small deviations in SO_4 concentrations.

Denitrification rate constants in the PPTs increased from 0.00 to 0.06 d^{-1} during the first 6 days to 0.17–0.83 d^{-1} afterwards at the different depths (Table 2), while denitrification rate constants increased from 0.0 to 0.5 d^{-1} at the start of the onset of ASTR operation to 0.1–>1 d^{-1} later on.

During the PPTs, denitrification rate constants likely increased as a result of microbial adaptation and bioaugmentation or anaerobic NO_3 reduction coupled to Fe-oxidation (Smith et al., 2017). Rivett et al. (2008) defines microbial adaptation as the 'lead time' needed before a microbial population is adapted to the new environmental conditions, which in this case is the injection of TDW containing high concentrations of NO_3: a new electron acceptor. Bioaugmentation refers to the addition of microbial cultures to enhance chemical transformations such as denitrification. Microbial adaptation and bioaugmentation are likely, as TDW (including microbiome) has not been injected before. Anaerobic NO_3 reduction coupled to Fe-oxidation could be occurring with increasing rate constants, as later samples contain a larger fraction of Fe-rich groundwater

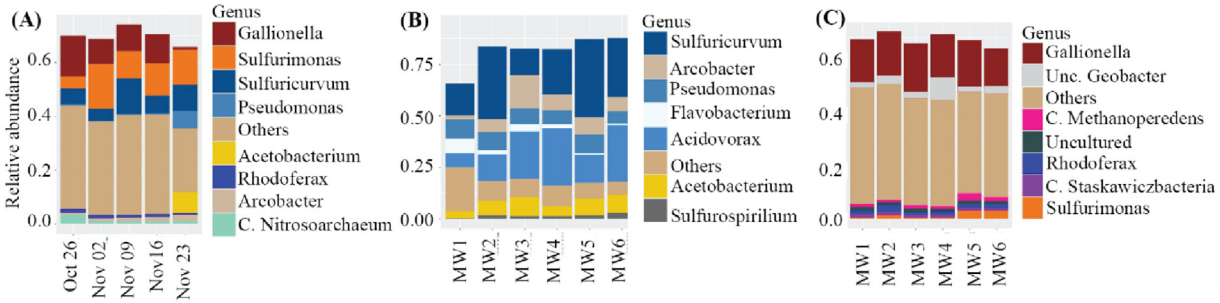

Fig. 5. Relative abundance of the bacterial communities present >1 % in (A) tile drainage water, (B) native groundwater, and (C) groundwater at the onset of the fall 2020 storage period. The abbreviation C. = Candidatus, and Unc. = uncultured.

Table 1
Spearman correlation of the microbiomes from the native aquifer (left table) and the fall 2020 storage period (right table) at the different depths compared to the average TDW microbiome obtained during the fall 2020 storage period and the native aquifer microbiome.

	Sample	ρ (TDW)
Native aquifer (2019) at:	MW1	0.49
	MW2	0.38
	MW3	0.43
	MW4	0.40
	MW5	0.42
	MW6	0.41

	Sample	ρ (TDW)	ρ (Native aquifer)
Fall 2020 storage period at:	MW1	0.83	0.38
	MW2	0.80	0.33
	MW3	0.82	0.33
	MW4	0.82	0.29
	MW5	0.82	0.32
	MW6	0.85	0.31

(Fe ~ 9–27 mg/L) due to mixing. During the onset of ASTR operation, anoxic NO_3 reduction coupled with Fe oxidation does not explain the increased denitrification rate constants, as Fe concentrations were substantially higher at the start of monitoring (8.4–37.3 mg/L) compared to the end (0.2–14.5 mg/L). Therefore, microbial adaptation and bioaugmentation seem the processes controlling the increased rate constants during the onset of ASTR operation, and this seems therefore also most likely to control rate constants during the PPTs. A similar quick adaptation of the microbial community was observed by Trudell et al. (1986), who performed a PPT with NO_3-rich water in a shallow unconfined sandy aquifer. Zero-order denitrification rate constants increased from 0.035 to 0.58 mg NO_3/L/d during the experiment which took about 15 days.

Deviating denitrification trends were observed at MW4 and MW6 during the onset of ASTR operation. At MW4, denitrification rate constants were high from the start and did not increase further, while a lower maximum rate constant was observed (0.25–0.5 d^{-1}) than at most other depths (>1 d^{-1}). No clear link was observed between electron donor contents/concentrations and the lower rate constant (S5). Microbial adaptation and bioaugmentation could have occurred faster here than at other depths, as (i) the permeability and the flow were highest at this depth and/or (ii) the maximum rate constant is lower at MW4 compared to the other depths and therefore it would take less time to reach this rate. Denitrification did start at all depths after arrival of the spreading front (1 pore volume) but not at MW6, where denitrification rate constants were negligible. This may be caused by the more saline conditions. A high salinity is known to inhibit denitrification. For example, Henze and Ucisik (2004) observed a 90 % reduction of the maximum denitrification rates when Cl concentrations were >5000 mg/L. In the current study, native groundwater Cl concentrations were >2500 mg/L at the start of operation and gradually decreased when the injected TDW was arriving. Cl concentrations decreased to <1500 mg/L at the end of the monitoring period.

Table 2
First-order denitrification rate constants (d^{-1}) obtained from the different monitoring approaches, and the mean temperature of the injected water.

	PPT		Onset of ASTR operation		Storage periods		
Mean temp. (°C)	10.6		11.7		~10	~14	~7
	k_{start}	k_{end}	k_{start}	k_{end}	$k_{winter\ '19}$	$k_{fall\ '20}$	$K_{spring\ '21}$
MW1	0.00	~0.29	0.25–0.5	>1	0.13	0.2	0.61
MW2	0.03	~0.83	0.25–0.5	>1	0.12	0.12	–
MW3	0.00	~0.54	0.25–0.5	>1	–	0.25	0.56
MW4	0.01	~0.22	0.25–0.5	0.25–0.5	0.15	0.12	0.12
MW5	0.01	~0.17	0.25–0.5	>1	0.14	0.12	0.12
MW6	0.06	~0.30	0	0.1–0.5	–	–	–

Kruisdijk and van Breukelen (2021) presented an overview of first-order denitrification rate constants determined in aquifers. Rate constants varied from 0.00049 to 18 d^{-1}, whereas they seemed generally higher, ranging from 0.1 to 10.1 d^{-1}, at hydrocarbon contaminated aquifers. Variation in hydrogeological aquifer properties, pH, microbial activity, and the abundance and reactivity of electron donors most likely cause the large range of observed denitrification rate constants (Einsiedl and Mayer, 2006; Korom, 1992). The rate constants as observed during operation in the current research are most comparable to those observed by Kruisdijk and van Breukelen (2021) (0.26–0.63 d^{-1}), who studied denitrification rate constants using PPTs at two depths during ASR operation at a research site <500 m away from the current ASTR field site.

4.1.2. Microbial adaptation versus bioaugmentation

Bioaugmentation besides microbial adaptation may have played a role in the temporal increase of the denitrification rate constants. The bacterial community of the TDW is substantially different from the native aquifer community, as shown in Section 3.5. We expect denitrifying bacteria in TDW, as the NO_3 and DOC concentrations were high and denitrification is commonly observed in soils of agricultural parcels (Hofstra and Bouwman, 2005; Seitzinger et al., 2006). Therefore, new types of bacteria are added to the aquifer (i.e. bioaugmentation), which can promote denitrification. The genera *Gallionella* (Korom, 1992; Matějů et al., 1992), *Sulfurimonas* (Frey et al., 2014; Zhang et al., 2009), *Sulfuricurvum* (Martínez-Santos et al., 2018; Saia et al., 2016), *Pseudomonas* (Carlson and Ingraham, 1983; Thomas et al., 1994), *Rhodoferax* (Jin et al., 2020; McIlroy et al., 2016), and *Arcobacter* (Heylen et al., 2006; Pishgar et al., 2019) are known to contain denitrifying species, and all show a relative abundance of >1 % in the TDW samples. Note that *Gallionella*, *Sulfurimonas*, and *Rhodoferax* appeared >1 % abundance in the aquifer during the fall 2020 storage period (Fig. 5C), while *Sulfuricurvum*, *Pseudomonas*, and *Arcobacter* were present >1 % in the native groundwater and in TDW, but were present below 1 % in the aquifer during the storage period.

Bioaugmentation is a proven practice for the degradation of chlorinated ethenes in groundwater (Lyon and Vogel, 2013; Steffan et al., 1999), but is also effective to enhance denitrification during water treatment (Shelly et al., 2021; Zhang et al., 2018). This implies that the microbial composition of the injected TDW can have a substantial influence on the denitrification rate constants. Injection of TDW, likely containing denitrifiers, may lead to a gradual built up of denitrifying biomass in the aquifer by attachment, and consequently increasing the estimated denitrification rate constants. From our results, a distinction between microbial adaptation and bioaugmentation cannot be made. A combination of both was likely responsible for the increased denitrification rate constants observed.

4.1.3. Lower rate constants during storage phases

The rate constants during storage periods were lower than those during the onset of ASTR operation. Rivett et al. (2008) stated that denitrification is largely depending on available electron donors and environmental conditions. The lower rate constants could suggest that electron donors are depleting over the course of ASTR operation. However, first-order rate constants are relatively stable during the different storage periods, which contradict this. Another condition influencing denitrification is temperature (Rivett et al., 2008). Temperature did not cause the variation in denitrification rate constants, as the mean injected water temperature was 11.7 °C during the onset of ASTR operation, which is similar to the temperature range observed during the storage periods (7–14 °C).

We suspect that the lower rate constants observed during the storage periods are related to the stagnant conditions, compared to the non-stagnant conditions generated by injection during ASTR operation. Stuyfzand et al. (2005) observed similarly that denitrification rates were higher during the injection phase than during stand-still at an ASR site in the southeast Netherlands. The induced flow likely enhances the exchange rate between the aquifer solid phase and injected TDW, which leads to higher denitrification rate constants. Note, that injection and storage alternate during ASTR

operation, and therefore denitrification rate constants are likely changing between injection and storage periods.

4.1.4. Intra-aquifer variations of denitrification

Intra-aquifer variations of first-order denitrification rate constants were deviating maximally a factor 5 at all depths during all monitoring approaches (Table 2). S5 presents the geochemical characteristics of the aquifer at the different well screen depths. Sedimentary organic carbon (SOC) and pyrite contents vary more than one order of magnitude. Generally, MW1, 2, and 3 have relatively high contents compared to MW4, 5, and 6. No clear associations between electron donor contents and denitrification rate constants were observed among the different depths. Previous studies obtained similar results and stated that oxidation rates are influenced more by SOC and pyrite reactivity compared to content (Kruisdijk and van Breukelen, 2021; Massmann et al., 2004).

4.2. Denitrification coupled to electron donors

Electron donors often related to denitrification are SOC and dissolved organic carbon (DOC), Fe^{2+}, and pyrite. NH_4 oxidation was not expected to be influential, as concentrations were low (0.13 ± 0.11 mg/L). Kruisdijk and van Breukelen (2021) coupled denitrification to a combination of mostly pyrite and SOC oxidation at an ASR system at <500 m distance from the current field site. Denitrification often results in distinctive water quality changes, which reflect the electron donors that oxidized (Korom et al., 2012; Kruisdijk and van Breukelen, 2021).

During the PPTs in the current study, water quality changes were not substantial enough to assess reductants coupled to denitrification, because only small concentrations of NO_3 were reduced (S2.1). During the onset of ASTR operation, SO_4 concentrations were substantially higher than those expected based on conservative mixing at all MWs (except of MW1), which indicates pyrite oxidation (S3.2; Fig. S4). Furthermore, DOC degradation/oxidation was probably observed because concentrations after arrival of the spreading front were lower than those injected and fitted considerably better to simulated degradation than sorption (for more information see S6). Pyrite and DOC oxidation do not need to relate to denitrification because also O_2 will oxidize them. Fe^{2+} oxidation was not observed during the onset of ASTR operation, because concentrations were instead mostly remarkably higher than expected based on conservative mixing (S3.2). This is probably related to reductive dissolution of Fe-hydroxides or the release of Fe^{2+} from cation exchange sites or pyrite oxidation. DOC and SOC oxidation results in an increased alkalinity. This is not clearly observed during the onset of ASTR operation (S3.2), although it could be that a potential increase in alkalinity is small and therefore hard to observe in the obtained data.

During the storage periods, SO_4 concentrations generally increased at all depths (S4.2), although at some depths decreasing or relatively stable concentrations were observed. At MW1, 3, and 5, SO_4 concentrations stabilized after NO_3 was depleted, which indicates a clear association between denitrification and pyrite oxidation. DOC and Fe^{2+} oxidation are not suggested by the stable DOC concentrations, and the increase of Fe^{2+} concentrations probably results from reductive dissolution of Fe-hydroxides or pyrite oxidation. Again, no clear increasing alkalinity is observed which could indicate DOC or/and SOC oxidation (S4.2). Fig. 6 shows the electrons released by the formation of SO_4 during pyrite oxidation versus the accepted electrons during denitrification. This was estimated by multiplying the molar difference in concentration of SO_4 and NO_3 between the start and end of the storage period with the electrons released/accepted (for more information see Kruisdijk and van Breukelen (2021)). The black linear line indicates a 1:1 ratio of released and accepted electrons, which suggests that all denitrification is related to pyrite oxidation. Some number of datapoints plot relatively close to this line, but the majority plot below it. This indicates that other oxidation processes are occurring besides the pyrite oxidation, like SOC or DOC oxidation.

4.3. Risks of injecting NO_3-rich tile drainage water

4.3.1. Risks of NO_3 contamination

This field study showed that denitrification occurred in the aquifer, and NO_3 is fully depleted in the aquifer if given enough retention time. Groundwater contamination risks of NO_3 are negligible in these circumstances, as (i) the lag-phase at the onset of ASTR operation was relatively short (6 days), and (ii) rate constants were not declining over time. Although this could still occur due to depletion of reductants over longer timescales or more intensive operation (Antoniou et al., 2013). Note that NO_3 in injection water is often not the only contamination risk. NO_3 is an indicator of anthropogenic contamination, which can also consist of other contaminants, such as pesticides and PO_4.

4.3.2. Risk of N_2O emissions

Nitrous oxide (N_2O) is an important greenhouse gas, which can accumulate in aquifers after denitrification (Jurado et al., 2017). In the current study, accumulated N_2O could be emitted to the atmosphere during ASTR abstraction. However, N_2O is generally transformed rapidly to nitrogen gas (N_2) (Rivett et al., 2008). Tiedje et al. (1982) stated that most denitrifying bacteria can complete the total pathway of denitrification from NO_3 to N_2. Denitrifying bacteria are not expected to limit this process within the aquifer, as previous research showed that they tend to be ubiquitous in aquifer systems (Rivett et al., 2008 and references therein). Nevertheless, N_2O transformation can be inhibited by high O_2 or NO_3 concentrations and/or low pH values (Blackmer and Bremner, 1978; Brady et al., 2008). Injected TDW has intermediate to high pH values (mostly between 7.0 and 7.5), and relatively high O_2 and NO_3 concentrations. As shown in the current study, O_2 and NO_3 are consumed relatively quickly, after which N_2O transformation will start. Boisson et al. (2013) studied the full reaction chain of denitrification reactions ($NO_3 \rightarrow NO_2 \rightarrow NO \rightarrow N_2O \rightarrow N_2$) in a fractured crystalline aquifer. They observed that the transformation of N_2O to N_2 is >200× faster than from NO_3 to NO_2 under anaerobic conditions. Therefore, N_2O accumulation and N_2O emissions during abstraction events are expected to be negligible.

4.4. Benefits of short timeframe in-situ monitoring approaches

In the current study, we performed several short (6–46 days) high-frequency in-situ monitoring approaches to study denitrification in an ASTR system, instead of the commonly used interpretation of operational monitoring data obtained from lower-frequency periodical monitoring of injected and abstracted water composition and the groundwater composition observed at monitoring wells (e.g., Antoniou et al., 2013; Barkow et al., 2021; Greskowiak et al., 2005). The presented approach enabled us to obtain denitrification rate constants before and at several moments during ASTR operation, instead of a best fit rate constant for an entire monitoring period (e.g., Barkow et al., 2021; Greskowiak et al., 2005; Vanderzalm et al., 2013). The PPT and the monitoring of the onset of ASTR operation are useful to assess denitrification in AS(*T*)R systems in which injection water quality varies over time, because its composition is monitored. The method used to monitor the onset of ASTR operation could be repeated to validate the higher rate constants expected during injection. Note that natural tracer concentrations of the injected water should be distinctively varying from concentrations in groundwater, in order to assess the arrival of the injected water, or alternatively an artificial tracer could be added.

The injected TDW composition was not monitored before the storage periods, but we assumed that it is stable over time. This assumption is not 100 % correct, as injected TDW composition changes slightly over time together with the NO_3 concentrations. This results in slightly heterogeneous NO_3 concentrations in the aquifer, which had negligible effects on the results of this study as convincing denitrification trends are observed during all storage periods. Nevertheless, the effect of variations in injected TDW composition should be considered during future studies. Furthermore, monitoring wells should be relatively close to the injection well, so

that travel times to these wells are not too long resulting in too low NO_3 concentrations resulting from denitrification at the start of the storage periods. The proposed methods can be a welcome addition or replacement to the standard operational monitoring and enables to assess the evolution of denitrification rate constants within the aquifer in more detail.

5. Conclusion

- A lag-phase was observed of approximately 6 days before denitrification started during the push-pull tests. First-order denitrification rate constants increased from 0.00 to 0.03 d^{-1} at the start to 0.17–0.83 d^{-1}. Quicker microbial adaptation and/or bioaugmentation occurred during the onset of ASTR operation, where first-order rate constants increased from between 0 and 0.5 to 0.1–>1 d^{-1} at the six investigated depths in the aquifer.
- Obtained denitrification rate constants were substantially higher during injection, in comparison to the 3 storage periods with stagnant conditions. These variations probably result from a lower exchange rate between the aquifer solid phase and injected TDW during storage compared to injection.
- NO_3 is fully reduced in maximum 20–40 days at all different aquifer depths, and no decrease in rate constants was observed during the injection of ~10.000 m^3 tile drainage water. Therefore, the risks of NO_3 contamination during injection of TDW are very low at this location, also taking into account the relatively short lag-phase initially observed.
- The short timeframe, high frequency in-situ field monitoring approaches can be used to examine denitrification lag-phases and denitrification rate constants before and during AS(*T*)R operation. The obtained information can be used to assess the risk of groundwater contamination by NO_3 during AS(*T*)R operation.

CRediT authorship contribution statement

Emiel Kruisdijk: Conceptualization, Methodology, Software, Formal analysis, Investigation, Writing – Original draft, Visualization **Pieter J. Stuyfzand:** Conceptualization, Writing – Review & Editing, Supervision **Boris M. van Breukelen:** Conceptualization, Methodology, Writing – Review & Editing, Supervision, Project administration, Funding acquisition.

Data availability

Data will be made available on request.

Declaration of competing interest

The authors declare that they have no known competing financial interests or personal relationships that could have appeared to influence the work reported in this paper.

Acknowledgements

This work was supported by the Netherlands Organisation for Scientific Research (NWO; Topsector Water Call 2016; project acronym AGRIMAR; contract number: ALWTW.2016.023) with co-funding from private partners Acacia Water B.V., Broere Beregening B.V., and Delphy B.V. We would like to thank Acacia Water B.V. for their contribution to the fieldwork; Vita Marquenie and David Weissbrodt for their contribution to the fieldwork and 16S rRNA analysis; and Patricia van den Bos and Jane Erkemeij for their contribution to the laboratory work.

Appendix A. Supplementary data

Supplementary data to this article can be found online at https://doi.org/10.1016/j.scitotenv.2022.157791.

References

Antoniou, E.A., van Breukelen, B.M., Putters, B., Stuyfzand, P.J., 2012. Hydrogeochemical patterns, processes and mass transfers during aquifer storage and recovery (ASR) in an anoxic sandy aquifer. Appl. Geochem. 27, 2435–2452.
Antoniou, E.A., Stuyfzand, P.J., van Breukelen, B.M., 2013. Reactive transport modeling of an aquifer storage and recovery (ASR) pilot to assess long-term water quality improvements and potential solutions. Appl. Geochem. 35, 173–186.
Appelo, C.A.J., Postma, D., 2004. Geochemistry, Groundwater and Pollution. CRC Press.
Barkow, I.S., Oswald, S.E., Lensing, H.-J., Munz, M., 2021. Seasonal dynamics modifies fate of oxygen, nitrate, and organic micropollutants during bank filtration — temperature-dependent reactive transport modeling of field data. Environ. Sci. Pollut. Res. 28, 9682–9700.
Bekins, B.A., Warren, E., Godsy, E.M., 1998. A comparison of zero-order, first-order, and monod biotransformation models. Groundwater 36, 261–268.
Blackmer, A.M., Bremner, J.M., 1978. Inhibitory effect of nitrate on reduction of N2O to N2 by soil microorganisms. Soil Biol. Biochem. 10, 187–191.
Blakey, N.C., Towler, P.A., 1988. The effect of Unsaturated/Saturated zone property upon the hydrogeochemical and microbiological processes involved in the migration and attenuation of landfill leachate components. Water Sci. Technol. 20, 119–128.
Boisson, A., de Anna, P., Bour, O., Le Borgne, T., Labasque, T., Aquilina, L., 2013. Reaction chain modeling of denitrification reactions during a push–pull test. J. Contam. Hydrol. 148, 1–11.
Bonte, M., van Breukelen, B.M., Stuyfzand, P.J., 2013. Temperature-induced impacts on groundwater quality and arsenic mobility in anoxic aquifer sediments used for both drinking water and shallow geothermal energy production. Water Res. 47, 5088–5100.
Bonte, M., Stuyfzand, P.J., van Breukelen, B.M., 2014. Reactive transport modeling of thermal column experiments to investigate the impacts of aquifer thermal energy storage on groundwater quality. Environ. Sci. Technol. 48, 12099–12107.
Brady, N.C., Weil, R.R., Weil, R.R., 2008. The Nature and Properties of Soils. Prentice Hall Upper Saddle River, NJ.
Breukelen, B.M.V., Prommer, H., 2008. Beyond the rayleigh equation: reactive transport modeling of isotope fractionation effects to improve quantification of biodegradation. Environ. Sci. Technol. 42, 2457–2463.
Camargo, J.A., Alonso, Á., 2006. Ecological and toxicological effects of inorganic nitrogen pollution in aquatic ecosystems: a global assessment. Environ. Int. 32, 831–849.
Carlson, C.A., Ingraham, J.L., 1983. Comparison of denitrification by Pseudomonas stutzeri, Pseudomonas aeruginosa, and Paracoccus denitrificans. Appl. Environ. Microbiol. 45, 1247–1253.
Einsiedl, F., Mayer, B., 2006. Hydrodynamic and microbial processes controlling nitrate in a fissured-porous karst aquifer of the Franconian alb, southern Germany. Environ. Sci. Technol. 40, 6697–6702.
Frey, C., Hietanen, S., Jürgens, K., Labrenz, M., Voss, M., 2014. N and O isotope fractionation in nitrate during chemolithoautotrophic denitrification by sulfurimonas gotlandica. Environ. Sci. Technol. 48, 13229–13237.
Ghafari, S., Hasan, M., Aroua, M.K., 2009. Effect of carbon dioxide and bicarbonate as inorganic carbon sources on growth and adaptation of autohydrogenotrophic denitrifying bacteria. J. Hazard. Mater. 162, 1507–1513.
Gorski, G., Dailey, H., Fisher, A.T., Schrad, N., Saltikov, C., 2020. Denitrification during infiltration for managed aquifer recharge: infiltration rate controls and microbial response. Sci. Total Environ. 727, 138642.
Greskowiak, J., Prommer, H., Vanderzalm, J., Pavelic, P., Dillon, P., 2005. Modeling of carbon cycling and biogeochemical changes during injection and recovery of reclaimed water at Bolivar, South Australia. Water Resources Research 41.
Haggerty, R., Schroth, M., Istok, J., 1998. Simplified method of"push-pull" test data analysis for determining in situ reaction rate coefficients. Ground Water 36, 314.
Henze, M., Ucisik, A.S., 2004. Biological denitrification of fertiliser wastewater at high chloride concentration. Water SA 30, 191–195.
Heylen, K., Vanparys, B., Wittebolle, L., Verstraete, W., Boon, N., Vos, P.D., 2006. Cultivation of denitrifying bacteria: optimization of isolation conditions and diversity study. Appl. Environ. Microbiol. 72, 2637–2643.
Hofstra, N., Bouwman, A.F., 2005. Denitrification in agricultural soils: summarizing published data and estimating global annual rates. Nutr. Cycl. Agroecosyst. 72, 267–278.
Hunter, W.J., 2003. Accumulation of nitrite in denitrifying barriers when phosphate is limiting. J. Contam. Hydrol. 66, 79–91.
Istok, J.D., 2012. Push-Pull Tests for Site Characterization. Springer Science & Business Media.
Jin, C.-Z., Zhuo, Y., Wu, X., Ko, S.-R., Li, T., Jin, F.-J., Ahn, C.-Y., Oh, H.-M., Lee, H.-G., Jin, L., 2020. Genomic and metabolic insights into denitrification, sulfur oxidation, and multidrug efflux pump mechanisms in the Bacterium rhodoferax sediminis sp. nov. Microorganisms 8, 262.
Jones, G.W., Pichler, T., 2007. Relationship between pyrite stability and arsenic mobility during aquifer storage and recovery in southwest Central Florida. Environ. Sci. Technol. 41, 723–730.
Jurado, A., Borges, A.V., Brouyère, S., 2017. Dynamics and emissions of N2O in groundwater: a review. Sci. Total Environ. 584–585, 207–218.
Korom, S.F., 1992. Natural denitrification in the saturated zone: a review. Water Resour. Res. 28, 1657–1668.
Korom, S.F., Schlag, A.J., Schuh, W.M., Kammer Schlag, A., 2005. In situ mesocosms: denitrification in the Elk Valley aquifer. Groundw. Monit. Remediat. 25, 79–89.
Korom, S.F., Schuh, W.M., Tesfay, T., Spencer, E.J., 2012. Aquifer denitrification and in situ mesocosms: modeling electron donor contributions and measuring rates. J. Hydrol. 432–433, 112–126.
Kowalenko, C., 1979. The influence of sulfur anions on denitrification. Can. J. Soil Sci. 59, 221–223.

Kruisdijk, E., van Breukelen, B.M., 2021. Reactive transport modelling of push-pull tests: a versatile approach to quantify aquifer reactivity. Appl. Geochem. 131, 104998.
Lyon, D.Y., Vogel, T.M., 2013. Bioaugmentation for groundwater remediation: An overview. In: Stroo, H.F., Leeson, A., Ward, C.H. (Eds.), Bioaugmentation for Groundwater Remediation. Springer, New York, New York, NY, pp. 1–37.
Martínez-Santos, M., Lanzén, A., Unda-Calvo, J., Martín, I., Garbisu, C., Ruiz-Romera, E., 2018. Treated and untreated wastewater effluents alter river sediment bacterial communities involved in nitrogen and sulphur cycling. Sci. Total Environ. 633, 1051–1061.
Massmann, G., Pekdeger, A., Merz, C., 2004. Redox processes in the oderbruch polder groundwater flow system in Germany. Appl. Geochem. 19, 863–886.
Matějů, V., Čižinská, S., Krejčí, J., Janoch, T., 1992. Biological water denitrification—a review. Enzym. Microb. Technol. 14, 170–183.
McIlroy, S.J., Starnawska, A., Starnawski, P., Saunders, A.M., Nierychlo, M., Nielsen, P.H., Nielsen, J.L., 2016. Identification of active denitrifiers in full-scale nutrient removal wastewater treatment systems. Environ. Microbiol. 18, 50–64.
Miettinen, H., Kietäväinen, R., Sohlberg, E., Numminen, M., Ahonen, L., Itävaara, M., 2015. Microbiome composition and geochemical characteristics of deep subsurface high-pressure environment, Pyhäsalmi mine Finland. Frontiers in Microbiology 6.
Muyzer, G., Waal, E.C.d., Uitterlinden, A.G., 1993. Profiling of complex microbial populations by denaturing gradient gel electrophoresis analysis of polymerase chain reaction-amplified genes coding for 16S rRNA. Appl Environ Microbiol 59, 695–700.
Oksanen, J., Blanchet, F.G., Kindt, R., Legendre, P., Minchin, P.R., O'hara, R., Simpson, G.L., Solymos, P., Stevens, M.H.H., Wagner, H., 2013. Package 'Vegan'. Community Ecology Package, Version 2, pp. 1–295.
Parkhurst, D.L., Appelo, C.A.J., 2013. Description of input and examples for PHREEQC version 3: a computer program for speciation, batch-reaction, one-dimensional transport, and inverse geochemical calculations. Techniques and Methods, p. 519 Reston, VA.
Pishgar, R., Dominic, J.A., Sheng, Z., Tay, J.H., 2019. Denitrification performance and microbial versatility in response to different selection pressures. Bioresour. Technol. 281, 72–83.
Prommer, H., Stuyfzand, P.J., 2005. Identification of temperature-dependent water quality changes during a deep well injection experiment in a pyritic aquifer. Environ. Sci. Technol. 39, 2200–2209.
Pyne, R.D.G., 1995. Groundwater Recharge and Wells: A Guide to Aquifer Storage Recovery. Routledge, New York, U.S.A.
RC, T., 2013. R: A Language and Environment for Statistical Computing.
Rivett, M.O., Buss, S.R., Morgan, P., Smith, J.W.N., Bemment, C.D., 2008. Nitrate attenuation in groundwater: a review of biogeochemical controlling processes. Water Res. 42, 4215–4232.
Rust, C.M., Aelion, C.M., Flora, J.R.V., 2000. Control of pH during denitrification in subsurface sediment microcosms using encapsulated phosphate buffer. Water Res. 34, 1447–1454.
Sáez, F., Pozo, C., Gómez, M.A., Martínez-Toledo, M.V., Rodelas, B., Gónzalez-López, J., 2006. Growth and denitrifying activity of Xanthobacter autotrophicus CECT 7064 in the presence of selected pesticides. Appl. Microbiol. Biotechnol. 71, 563–567.
Saia, F.T., Souza, T.S., Duarte, R.T.D., Pozzi, E., Fonseca, D., Foresti, E., 2016. Microbial community in a pilot-scale bioreactor promoting anaerobic digestion and sulfur-driven denitrification for domestic sewage treatment. Bioprocess Biosyst. Eng. 39, 341–352.
Schmidt, C.M., Fisher, A.T., Racz, A.J., Lockwood, B.S., Huertos, M.L., 2011. Linking denitrification and infiltration rates during managed groundwater recharge. Environ. Sci. Technol. 45, 9634–9640.
Schnell, S., Mendoza, C., 1997. Closed form solution for time-dependent enzyme kinetics. J. Theor. Biol. 187, 207–212.
Seitzinger, S., Harrison, J.A., Böhlke, J.K., Bouwman, A.F., Lowrance, R., Peterson, B., Tobias, C., Drecht, G.V., 2006. Denitrification across landscapes and waterscapes: a synthesis. Ecol. Appl. 16, 2064–2090.
Shelly, Y., Kuk, M., Menashe, O., Zeira, G., Azerrad, S., Kurzbaum, E., 2021. Nitrate removal from a nitrate-rich reverse osmosis concentrate: superior efficiency using the bioaugmentation of an acinetobacter biofilm. J. Water Process Eng. 44, 102425.
Sheng, Z., 2005. An aquifer storage and recovery system with reclaimed wastewater to preserve native groundwater resources in El Paso, Texas. J. Environ. Manag. 75, 367–377.
Shu, D., He, Y., Yue, H., Wang, Q., 2016. Metagenomic and quantitative insights into microbial communities and functional genes of nitrogen and iron cycling in twelve wastewater treatment systems. Chem. Eng. J. 290, 21–30.
Smith, R.L., Kent, D.B., Repert, D.A., Böhlke, J.K., 2017. Anoxic nitrate reduction coupled with iron oxidation and attenuation of dissolved arsenic and phosphate in a sand and gravel aquifer. Geochim. Cosmochim. Acta 196, 102–120.
Steffan, R.J., Sperry, K.L., Walsh, M.T., Vainberg, S., Condee, C.W., 1999. Field-scale evaluation of in situ bioaugmentation for remediation of chlorinated solvents in groundwater. Environmental Science & Technology 33, 2771–2781.
Stuyfzand, P.J., Bunnik, J., Medema, G., Vogelaar, A., Wakker, J., Verheijden, S., 2005. Water quality changes, clogging and pathogen transport during deep well injection in the South-East Netherlands (DIZON). Water Quality Improvements During Aquifer Storage and Recovery, pp. 77–103.
Thomas, K.L., Lloyd, D., Boddy, L., 1994. Effects of oxygen, pH and nitrate concentration on denitrification by pseudomonas species. FEMS Microbiol. Lett. 118, 181–186.
Tiedje, J.M., Sexstone, A.J., Myrold, D.D., Robinson, J.A., 1982. Denitrification: ecological niches, competition and survival. Antonie Van Leeuwenhoek 48, 569–583.
Trudell, M.R., Gillham, R.W., Cherry, J.A., 1986. An in-situ study of the occurrence and rate of denitrification in a shallow unconfined sand aquifer. J. Hydrol. 83, 251–268.
Vanderzalm, J.L., Page, D.W., Barry, K.E., Dillon, P.J., 2013. Application of a probabilistic modelling approach for evaluation of nitrogen, phosphorus and organic carbon removal efficiency during four successive cycles of aquifer storage and recovery (ASR) in an anoxic carbonate aquifer. Water Res. 47, 2177–2189.
Vanderzalm, J.L., Page, D., Regel, R., Ingleton, G., Nwayo, C., Gonzalez, D., 2020. Nutrient transformation and removal from treated wastewater recycled via aquifer storage and recovery (ASR) in a carbonate aquifer. Water Air Soil Pollut. 231, 65.
Wolfe, A.H., Patz, J.A., 2002. Reactive nitrogen and human health:acute and long-term implications. AMBIO J. Hum. Environ. 31, 120–125 126.
Zhang, M., Zhang, T., Shao, M.F., Fang, H.H.P., 2009. Autotrophic denitrification in nitrate-induced marine sediment remediation and sulfurimonas denitrificans-like bacteria. Chemosphere 76, 677–682.
Zhang, S., Sun, X., Wang, X., Qiu, T., Gao, M., Sun, Y., Cheng, S., Zhang, Q., 2018. Bioaugmentation with diaphorobacter polyhydroxybutyrativorans to enhance nitrate removal in a poly (3-hydroxybutyrate-co-3-hydroxyvalerate)-supported denitrification reactor. Bioresour. Technol. 263, 499–507.
Zuurbier, K.G., Hartog, N., Stuyfzand, P.J., 2016. Reactive transport impacts on recovered freshwater quality during multiple partially penetrating wells (MPPW-)ASR in a brackish heterogeneous aquifer. Appl. Geochem. 71, 35–47.